ResearchGate

See discussions, stats, and author profiles for this publication at: https://www.researchgate.net/publication/231639678

Theoretical Investigation of OCN− Charge-Transfer Complexes in Condensed-Phase Media: Spectroscopic Properties in Amorphous Ice

ARTICLE *in* THE JOURNAL OF PHYSICAL CHEMISTRY A · JULY 2004

Impact Factor: 2.69 · DOI: 10.1021/jp048763m

CITATIONS
16

READS
16

2 AUTHORS, INCLUDING:

David E Woon
University of Illinois, Urbana-Champaign
104 PUBLICATIONS **11,590** CITATIONS

SEE PROFILE

Available from: David E Woon
Retrieved on: 25 January 2016

Theoretical Investigation of OCN^- Charge-Transfer Complexes in Condensed-Phase Media: Spectroscopic Properties in Amorphous Ice

Jin-Young Park* and David E. Woon

Molecular Research Institute, 2495 Old Middlefield Way, Mountain View, California 94043

Received: March 19, 2004; In Final Form: May 28, 2004

Density functional theory (DFT) calculations of cyanate (OCN^-) charge-transfer complexes were performed to model the "XCN" feature observed in interstellar icy grain mantles. OCN^- charge-transfer complexes were formed from precursor combinations of HNCO or HOCN with either NH_3 or H_2O. Three different solvation strategies for realistically modeling the ice matrix environment were explored, including (1) continuum solvation, (2) pure DFT cluster calculations, and (3) an ONIOM DFT/PM3 cluster calculation. The model complexes were evaluated by their ability to reproduce seven spectroscopic measurements associated with XCN: the band origin of the OCN^- asymmetric stretching mode, shifts in that frequency due to isotopic substitutions of C, N, O, and H, plus two weak features. The continuum solvent field method produced results consistent with some of the experimental data but failed to account for other behavior due to its limited capacity to describe molecular interactions with solvent. DFT cluster calculations successfully reproduced the available spectroscopic measurements very well. In particular, the deuterium shift showed excellent agreement in complexes where OCN^- was fully solvated. Detailed studies of representative complexes including from two to twelve water molecules allowed the exploration of various possible solvation structures and provided insights into solvation trends. Moreover, complexes arising from cyanic or isocyanic acid in pure water suggested an alternative mechanism for the formation of OCN^- charge-transfer complexes without the need for a strong base such as NH_3 to be present. An extended ONIOM (B3LYP/PM3) cluster calculation was also performed to assess the impact of a more realistic environment on HNCO dissociation in pure water.

1. Introduction

Solvation is a fundamental issue in condensed-phase chemistry. It is a minor or major theme in fields ranging from biological, atmospheric, and environmental science to chemical manufacturing and nanotechnology. Aqueous solvation plays a role in many biochemical processes, such as enzymatic reactions,[1,2] protein folding,[3−7] and pharmacology.[8,9] Also, much of environmental chemistry is dominated by solvent−solute interactions, which often occur at heterogeneous boundaries, as in the case of the adsorption and degradation of pollutant molecules at solid−water interfaces.[10−14] Solution behavior is even relevant in astrochemistry, where processes confined on or within the icy mantles that form around dust particles in the interstellar medium (ISM) may be considerably different from gas-phase behavior.[15] While water is absolutely essential for terrestrial life, it's still an open question as to how critical and unique the role of water is for life in the universe at large.[16]

Solvation behavior depends upon the strength of the interactions between solvent/matrix molecules and solute species in various possible forms and the degree to which the cost of changing form is offset by more favorable interactions. Charge-transfer (CT) pairs, the subject of the present work, interact more energetically with water than their neutral parent species, but if the transfer is to happen, the gain due to stronger intermolecular interactions must exceed the cost of rearranging chemical bonds to form the new species. From a thermodynamic perspective, the disruption of pure water structure by solvent−solute interactions increases entropy and consequentially lowers the free energy.[17] This favorable change of free energy in solvation arises from the unique properties of condensed-phase water.

In modeling some of the processes that occur in water or ice with quantum chemistry, it is absolutely essential to include explicit water molecules that play a direct, chemical role.[18−21] However, under other circumstances, embedding the minimal set of molecular moieties in an approximate continuum solvent field is sufficient. The net solvent effect upon solute molecules is a combination of short-range interactions with water molecules in the first and second coordination shells plus the long-range interaction with the bulk matrix, which is mediated through the dielectric constant. The present work provides an instructive opportunity to compare and contrast different strategies for modeling the solvation behavior of CT pairs in ice.

Under the extremely low pressures and temperatures found in the ISM, H_2O can exist in both amorphous and crystalline forms of ice. At the temperatures where icy grain mantles form (10−20 K), the dominant morphology is high-density amorphous ice, with other impurity molecules trapped in the ice matrix.[22] Many of these molecules are small neutral organic species. While it has been known for many years that gas-phase chemistry in the ISM is dominated by ion−molecule reactions,[23−26] it is only recently that experimental studies[27,28] of photoprocessed astrophysical ice analogues have demonstrated the possibility of ion-rich ices. We have reported theoretical studies of ion generation in ices via photoionization elsewhere.[28,29] The focus of the present work is the facile formation of charge-transfer complexes from neutral precursors in astrophysical ices.

* Corresponding author. E-mail: jyp68@purisima.molres.org.

10.1021/jp048763m CCC: $27.50 © 2004 American Chemical Society
Published on Web 07/09/2004

As a result of experimental studies,[30,31] $OCN^- - NH_4^+$ charge-transfer complexes arising from HNCO and NH_3 have been proposed as the carrier for the so-called XCN feature at 2165 cm^{-1} (4.62 μm) that is observed in IR spectra of various interstellar objects.[30,32−36] Theoretical treatments by Raunier et al.[37−39] and preliminary work we reported recently[40] confirm that this is a very plausible candidate for the XCN carrier, although related OCN^- CT complexes may also be possible candidates. The hypothesis that OCN^- in ice is responsible for the XCN feature was advanced more than 15 years ago,[41] though other RCN or RNC species have also been explored.[42] Many experimental efforts[30,41,43−51] have reproduced the XCN feature from starting materials such as $CO-NH_3$, which supported the OCN^- conjecture. Also, measured isotope shifts for O, C, and N are consistent with the behavior of the OCN^- asymmetric stretching mode. However, confirmation of the OCN^- hypothesis was hindered by two issues: how could OCN^- form in ice at cryogenic temperatures, and why is a small but real deuterium isotope shift[45,46,50] (-8 cm^{-1}) observed in experimental studies? Recognition[39] that CT complexes account for the formation of OCN^- resolved the first issue, with theoretical work[40] demonstrating that this is a barrierless process if parents such as HNCO and NH_3 are situated adjacent to one another and embedded within an ice matrix. Also, the calculations reproduced the measured D shift, which was found to arise from small changes in the intermolecular interactions between OCN^- and its various near neighbors. The theoretical work thoroughly confirmed the experimental observations while providing additional insight.

Raunier and co-workers have recently reported several interrelated studies on OCN^- behavior in ices.[37−39] In the initial paper, they characterized the formation of the XCN feature when HNCO was either co-deposited with NH_3 in a 1:10 ratio at cryogenic temperatures or deposited on the surface of pure ammonia ice.[39] The $OCN^- - NH_4^+$ complex was found to form spontaneously during co-deposition at 10 K. When HNCO was adsorbed on the surface of an amorphous NH_3 thin film, the feature was not observed until the temperature was increased to 90 K, and the intensity was weaker than that in the co-deposition case. These experiments were supplemented with quantum chemical calculations of $HNCO-(NH_3)_n$ clusters, in which it was found that spontaneous proton transfer from HNCO to NH_3 requires at least three near-neighbor ammonia molecules. In the second paper, they reported that OCN^- again formed when HNCO was co-deposited with water or adsorbed on an H_2O ice surface once the temperature was increased to 110 K.[38] No NH_3 was present, suggesting that OCN^- CT complexes could form with different countercations. However, van Broeckhuizen, Keane, and Schutte[52] did not observe the formation of the 4.62 μm feature when they performed a similar experiment, in which a 14:1 H_2O/HNCO ice was only thermally processed, though the feature was observed when the ice was photoprocessed as well. As in their first study, Raunier and co-workers performed calculations in order to understand why their experimental results did not show any evidence of OCN^- without heating. They estimated the activation energy for proton transfer from isocyanic acid to water on an ice surface to be 10.0 kcal/mol. In the latest paper, they summarized and compared the reactivity of HNCO with ammonia in three different experiments: trapped in an argon matrix, co-deposited with NH_3, and adsorbed on surfaces of NH_3 ice. Quantum chemical calculations were once again performed to gain insight into their various results in co-deposition and adsorption experiments.[37]

Our studies differ from those of Raunier and co-workers in several ways. While they explored both water and ammonia ices, we have focused entirely on water ice, which is most relevant to the ISM. Likewise, where Raunier and co-workers emphasized surface reactions, our theoretical studies have focused on fully embedded CT complexes. Also, we have investigated another possible parent molecule, HOCN, and have characterized cases where the counterion is H_3O^+ rather than NH_4^+ in order to understand how much variation is possible in the spectroscopic properties of $OCN^- - X^+$ CT complexes.

Our preliminary study[40] highlighted the largest cluster calculations and part of the variation issue mentioned above. The present work more fully details calculations on various structures with increasing water coordination, explores various solvation models, and also addresses the comparison between $OCN^- - NH_4^+$ and $OCN^- - H_3O^+$ CT complexes. We characterized the various possible CT complexes arising from HNCO and HOCN paired with either NH_3 or H_2O using quantum calculations at the density functional theory (DFT) B3LYP level and investigated three different solvation models to account for the ice matrix. While HNCO is the best candidate for the parent of OCN^- based on its known presence in the ISM,[53−55] isomeric cyanic acid HOCN is another plausible parent molecule and, in fact, yields a CT complex with very similar spectroscopic properties. Likewise, we sought to determine if H_2O, as a weaker base than NH_3, could also induce the formation of CT complexes at cryogenic temperatures.

Three solvent models of varying complexity were explored. The simplest model investigated was the continuum solvent field method, which accounts approximately for bulk solvent effects. It performed reasonably well, but the neglect of explicit short-range interactions with solvent molecules introduces critical limitations and inaccuracy. Most of the present work employed pure DFT cluster calculations, where the approximate field was replaced with explicit water molecules to create a realistic short-range environment. By examining trends as the number of water molecules was increased from two to twelve, we ascertained the degree of coordination that successfully reproduces the reported spectroscopic measurements, including isotope shifts. Finally, a DFT/PM3 ONIOM calculation was used in one instance to attempt to address an issue not resolved by pure DFT calculations: expanding to a cluster with 27 water molecules incorporated bulk structural features not present in smaller clusters.

2. Computational Methodology

All calculations were performed with the GAUSSIAN 98 suite[56] of electronic structure programs. Hessian calculations, including isotopic substitutions, were performed for optimized structures to determine the frequency associated with the XCN feature, the asymmetric OCN stretching mode, as well as the frequencies of the weaker OCN symmetric stretching and bending modes. For isotopic substitution cluster calculations, all of the atoms of each element (C, N, O, and H) were completely replaced with their respective isotopes in order to compare with the experimental data of Bernstein et al.[46] Calculated frequencies were scaled by 0.9692. While this scaling factor is similar to values in widespread use, it was specifically derived from comparisons between computed and experimental values for the OCN asymmetric stretching frequencies of HNCO, HOCN, and OCN^-, for which data were taken from the NIST Chemistry WebBook database.[63]

As mentioned in the Introduction, three different solvation models of varying complexity were investigated for treating the formation and spectroscopic properties of CT complexes: (i) At the simplest level, the bulk ice environment was

approximated with self-consistent reaction field calculations performed using the polarized continuum model[64] (PCM), with SOLVENT=WATER, or the isodensity-surface polarized continuum model[65] (IPCM), with a dielectric constant of 78.5. The behavior of HNCO and HOCN paired with either NH_3 or H_2O and no additional water was examined with either optimizations or potential-energy scans. (ii) The majority of the present work consisted of pure DFT cluster calculations at the B3LYP level[66,67] using 6-31+G** basis sets,[68,69] with explicit water molecules replacing the approximate solvent field. DFT has established itself as a reliable methodology that is very appropriate for the study of charge-transfer behavior and vibrational-mode calculations as exemplified by various recent studies.[57−62] In particular, Ding and Laasonen[62] recently reported a study of the deprotonation of sulfuric acid using DFT cluster calculations that parallels the present work in many respects. They found that DFT compared quite adequately with MP2 and experimental behavior. We will describe the results of several MP2 calculations for small clusters to demonstrate that DFT is quite suitable for addressing this work. Complexes of HNCO and HOCN paired with NH_3 and solvated with two to twelve explicit water molecules were built by adding water molecules one by one around the optimized structures of HNCO (or HOCN) and NH_3 in the gas phase. Multiple minima were identified for cases when two to six water molecules were present: the structures presented in section 4 were selected to be representative, not exhaustive. Optimized structures and calculated spectroscopic properties of $OCN^-{-}NH_4^+$ CT complexes were compared to determine the most realistic solvation environment. As reported in our preliminary paper,[40] $12H_2O$ $OCN^-{-}NH_4^+$ CT complexes with full coordination around OCN^- and NH_4^+ were found to yield excellent agreement with the available experimental spectroscopic data. By replacing NH_3 with H_2O in the largest complexes, we were able to study the tendency of the two acids to dissociate into OCN^- and H_3O^+ in a pure aqueous environment. Finally, $15H_2O$ OCN^- anion complexes were also optimized to represent the situation where OCN^- is well isolated by solvent from any counterions. Comparing the optimized structures and calculated frequencies for the extended family of OCN^- complexes revealed the range of variation that is possible in the XCN spectroscopic feature. (iii) An ONIOM calculation was performed to study the dissociation of HNCO in water. A two-level model was used, with the "high" model consisting of HNCO and nine water molecules treated at the B3LYP/6-31+G** level. This was coupled with a "low" model of HNCO with 27 water molecules treated at the PM3 level. In this version of ONIOM, the coupling mostly serves to provide geometric constraints on the hydrogen bonding network. Unfortunately, the high model does not experience the electronic polarization arising from the additional water molecules present in the low model.

3. OCN^- Complex Formation Modeled with IPCM and PCM Calculations

The simplest computational approach for modeling the formation of CT pairs employed in the current study involved embedding the interacting molecules in a continuum dielectric field with no explicit solvent molecules present. The formation of $OCN^-{-}NH_4^+$ and $OCN^-{-}H_3O^+$ complexes was investigated by subjecting pairings of HNCO or HOCN with NH_3 or H_2O to both IPCM and PCM solvent fields. The results illustrate both the merits and limitations of the continuum solvation approach.

Due to the restriction to single-point energy calculations, the IPCM method is of limited usefulness in the study of the formation of CT complexes and their spectroscopic properties. However, IPCM calculations can be used to contrast gas-phase and solvated behavior qualitatively. Potential-energy surfaces were generated by moving the H from the acid across to the N or O of NH_3 or H_2O, respectively. Figure 1 depicts a representative case: the conversion of $HNCO{-}NH_3$ to $OCN^-{-}NH_4^+$. A grid of points was generated by fixing the intermolecular r_{NN} distance at incremental values between 2.5 and 3.1 Å and then stepping the H a fraction of the distance between the two N atoms such that N−H bond lengths of 1.0 Å were present at the beginning and conclusion of the transit. The H and two N atoms were kept collinear. At each grid point, the remaining internal coordinates were optimized at the MP2/6-31+G** level. This was followed by a single-point IPCM-MP2/6-31+G** calculation. The gas-phase surface, Figure 1a, exhibits the single expected minimum for the weakly bound complex between HNCO and NH_3. By contrast, the IPCM surface, Figure 1b, exhibits two minima, one for the neutral molecules and a second, more stable minimum for the $OCN^-{-}NH_4^+$ CT complex. A shallow transition state separates the minima. Similar studies were performed for $HOCN{-}NH_3$ and both $HNCO{-}H_2O$ and $HOCN{-}H_2O$, and analogous behavior was observed. While the results are only of qualitative value, it does illustrate how much the solvent field stabilizes the ion pair relative to gas-phase behavior.

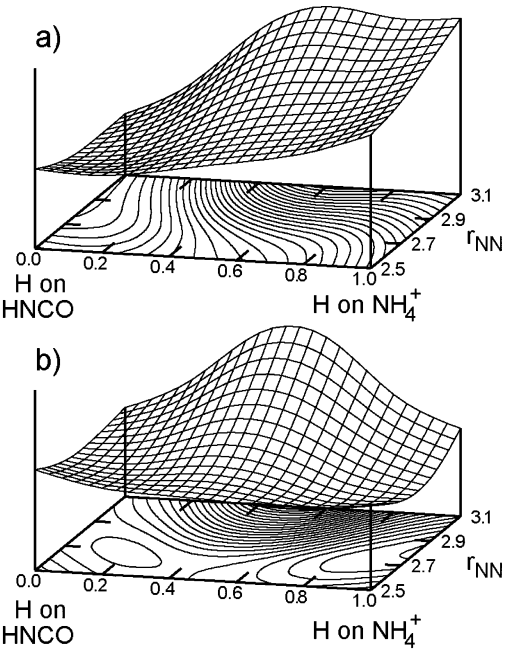

Figure 1. Potential-energy surfaces for H^+ migrating between HNCO and NH_3. (a) Gas phase. (b) Embedded within an IPCM continuum solvation field.

PCM calculations are of greater utility for examining spectroscopic behavior of ice-bound molecules and CT complexes due to the availability of optimizations and numerical second derivatives. Figure 2 depicts optimized PCM-B3LYP/6-31+G** structures for the various stationary points that were identified. While there is a minimum for neutral $HNCO{-}NH_3$, the transition state is only about 0.1 kcal/mol above the minimum. There is no neutral minimum for $HOCN{-}NH_3$. Thus, PCM calculations indicate that both acids readily deprotonate to OCN^- in the presence of a strong base such as NH_3. However, when NH_3 is replaced with H_2O, PCM calculations predict that the acids remain intact and are not deprotonated, a finding that is contradicted by cluster calculations that will be discussed in section 4.

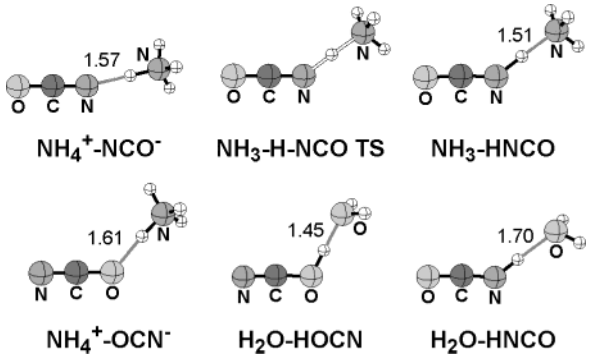

Figure 2. Optimized PCM structures for interactions of HNCO and HOCN with either NH_3 or H_2O.

TABLE 1: Scaled PCM-B3LYP/6-31+G Frequencies and Isotopic Shifts for the OCN^- Asymmetric Stretching Mode**

	frequency or shift (cm^{-1})		
property	from HNCO	from HOCN	OCN^-
ν_3	2166	2167	2141
$\Delta\nu_3$ ($^{12}C \rightarrow {}^{13}C$)	−54	−57	−57
$\Delta\nu_3$ ($^{14}N \rightarrow {}^{15}N$)	−16	−19	−18
$\Delta\nu_3$ ($^{16}O \rightarrow {}^{18}O$)	−6	−5	−7
$\Delta\nu_3$ ($^{1}H \rightarrow {}^{2}H$)	+12	+14	

Scaled frequencies and isotope shifts for the $OCN^- - NH_4^+$ CT structures arising from HNCO and HOCN as well as for isolated OCN^- are given in Table 1. The values of ν_3 are essentially the same if NH_4^+ is present at either end of OCN^- and are in very good agreement with the experimental value of 2165 cm^{-1}. Without NH_4^+, ν_3 is shifted by about −25 cm^{-1}. The C, N, and O isotope shifts are all reasonably close to the values reported by Bernstein et al.,[46] but the deuterium shift is in the wrong direction. The cluster calculations described below indicate that the D shift is delocalized and requires explicit treatment of solvent interactions representing the local coordination environment, a factor for which the PCM polarization field cannot account. While there are problems, the PCM method can be useful for modeling some aspects of CT behavior.

4. OCN^- Complex Formation Modeled with Explicit Water: DFT Calculations

4.1. $OCN^- - NH_4^+$ CT Complexes in Water Clusters. In this section we will discuss $OCN^- - NH_4^+$ CT complexes, which were generated by optimizing complexes of NH_3 with either HNCO or HOCN in the presence of various numbers of explicit water molecules via DFT calculation. Clusters with up to twelve H_2O molecules were characterized, with the aim of saturating the coordination sites around $OCN^- - NH_4^+$. The H_2O to NH_3 ratio of our largest cluster size corresponds roughly to the water-rich 10:1 ratio reported in a recent analysis of the composition of the polar-phase ices of protostellar objects such as W33A and NGC 7538 IRS 9.[70]

Figure 3 depicts optimized B3LYP/6-31+G** structures of $OCN^- - NH_4^+$ CT complexes arising from HNCO and NH_3 with two, three, four, six, eight, and twelve water molecules. The complexes fall into two groups, contact ion pair (CIP) and solvent-separated pair (SSP) structures, depending on whether there is direct contact between OCN^- and NH_4^+. The figure only shows complexes formed from HNCO and NH_3: the analogous HOCN complexes are quite similar, aside from reversing the orientation of OCN^- from the HNCO case. MP2 calculations were also performed for HNCO in small complexes having two to four water molecules. Both methods exhibited the same behavior in charge transfer as a function of the amount

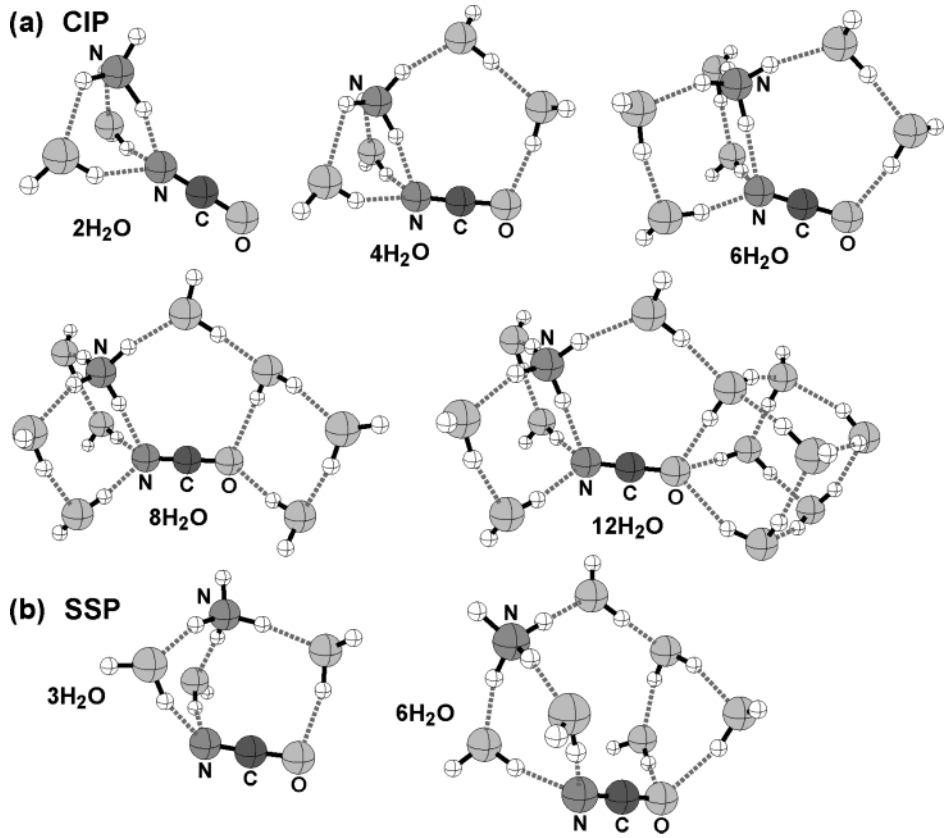

Figure 3. Optimized pure DFT structures for $OCN^- - NH_4^+$ from $HNCO - NH_3$ complexes solvated with various numbers of explicit water molecules. Similar structures were obtained from $HOCN - NH_3$, with OCN^- reversed. The numbers of water molecules are shown under the structures in the figure. (a) Contact ion pair (CIP) complexes. (b) Solvent-separated pair (SSP) complexes.

TABLE 2: Scaled Frequencies and Isotopic Shifts of OCN^- Complexes

					isotope shifts of ν_3					
parents	structure type[a]	N[b]	ν_3 of OCN^-	intensity of ν_3	^{18}O	^{15}N	^{13}C	D	ν_2 of OCN^-	ν_1 of OCN^-
$HNCO-NH_3$	CIP	12	2181	2.59×10^{-16}	−9	−16	−59	−7	618	1260
		8	2178	2.30×10^{-16}	−9	−15	−60	−19	627	1269
		6	2171	2.23×10^{-16}	−11	−15	−60	−6	628	1275
		4	2167	2.17×10^{-16}	−10	−15	−59	4	618	1270
		2	2207	1.26×10^{-16}	−13	−12	−58	−15	636	1310
	SSP	6	2182	1.88×10^{-16}	−8	−17	−59	−19	624	1254
		3	2166	3.97×10^{-16}	−9	−16	−59	−44	629	1303
$HOCN-NH_3$	CIP	12	2202	2.00×10^{-16}	−6	−19	−58	−13	610	1219
		8	2218	1.58×10^{-16}	−7	−23	−60	4	587	1209
		6	2215	1.29×10^{-16}	−5	−21	−58	−24	586	1189
		4	2202	1.26×10^{-16}	−5	−20	−57	42	606	1195
		2	2211	1.19×10^{-16}	−4	−22	−54	18	571	1149
	SSP	6	2199	1.49×10^{-16}	−6	−19	−58	−15	588	1244
		3	2189	1.05×10^{-16}	−5	−19	−57	19	586	1206
$HNCO-H_2O$	SSP	12	2187	2.58×10^{-16}	−9	−16	−60	−10	613	1267
$HOCN-H_2O$	SSP	12	2206	2.01×10^{-16}	−6	−19	−58	−9	597	1221
OCN^-	ION[c]	15	2194	2.28×10^{-16}	−5	−17	−57	−6	610	1227
OCN^-	ION[c]	15	2184	2.16×10^{-16}	−8	−18	−60	−15	617	1253
experimental data[d]			2165	1.3×10^{-16}	−9	−19	−58	−8	630	1296

[a] CIP: contact ion pair. SSP: solvent-separate pair. ION: isolated ion. [b] Number of waters added as solvent. [c] Two OCN^- anion complexes with nearly identical water structures were optimized. See text. [d] XCN band origin from Lacy et al.,[43] intensity of ν_3 from van Broekhuizen et al.,[52] isotope shifts of ν_3 from Bernstein et al.,[46] and ν_1 and ν_2 of OCN^- from Schutte and Greenberg.[48]

of water present. Likewise, the structural parameters and frequencies are very similar. For example, hydrogen bond lengths in the DFT and MP2 $4H_2O$ clusters differ by no more than 0.02 Å, and the weak bond angles vary by less than 2°. There are also only slight differences (~0.01 Å) in the chemical bond lengths of OCN^- and the other molecular moieties. On the basis of these comparisons, it is evident that DFT is performing as well as MP2 in describing the structures.

Very little water is needed to stabilize the CT products for the reactions of either HNCO or HOCN with NH_3. While proton transfer in the $2H_2O$ complex of HNCO is not spontaneous and there is a minimum for the neutral species, the energy barrier is very small.[71] For complexes with three or more waters, proton transfer is spontaneous, and there is no minimum for the neutrals. In the HOCN case, deprotonation is more favorable, with spontaneous proton transfer occurring with just two waters. The tendency for HOCN to be deprotonated more readily than HNCO is also observed in the pure-water case discussed below.

All CIP structures have a direct hydrogen bond between OCN^- and NH_4^+. The first several waters cluster around NH_4^+, completing its first coordination shell while bridging across to OCN^-. The two additional waters in the $6H_2O$ structures serve to remove strain from two tight loops in the $4H_2O$ complexes. In the two largest cluster sizes, water coordination fills out around the other initially exposed end of OCN^-. Completing the coordination around OCN^- required us to construct the cuboid cage of seven interlocked waters that is present in the $12H_2O$ structures. While somewhat artificial compared to what is likely found in an amorphous ice matrix, these are the smallest structures identified in this work with full coordination around both ions.

In the process of searching for CIP structures, SSP structures with $3H_2O$ and $6H_2O$ were found. After the proton transferred during the initial optimization steps, the NH_4^+ and H_2O molecules continued to rearrange to produce the SSP structure. Water molecules moved between the cation and anion, separating them with bridging hydrogen bonds. This development was of pragmatic value, given that SSP structures evolve in real systems and are also of interest in characterizing the range of behavior of the OCN^- asymmetric stretch. In section 4.3, we have also considered the limiting case, where OCN^- is essentially isolated.

Considering the detailed structures, we find the CN and CO bond lengths of OCN^- showed consistent trends in all complexes. The value of r_{CN} tended to remain constant, at 1.20 Å for HNCO and 1.18 Å for HOCN, while r_{CO} shifted slightly as the number of water molecules was increased from two to twelve; r_{CO} changed by about 0.03 Å in both cases, increasing from 1.19 to 1.22 Å for HNCO and decreasing from 1.27 to 1.24 Å for HOCN. The hydrogen bond between NH_4^+ and OCN^- in the CIP structures lengthened considerably as water was added, increasing from around 1.5 Å in the $2H_2O$ complexes to more than 1.9 Å in the $12H_2O$ complexes. The range of other hydrogen bonds with water molecules varies from 1.80 to 2.10 Å. The charge separation within the OCN^- molecule also increased with cluster size. In the $12H_2O$ HNCO case, the Mulliken charges are −0.79 for O, 0.87 for C, and −1.02 for N, an approximately quadrupolar charge distribution. In the corresponding HOCN structure, the charges are −0.84 for O, 0.80 for C, and −0.89 for N, indicating that NH_4^+ polarizes OCN^- to a slightly different extent when it is coordinated to O rather than N.

Scaled frequency results, including the isotope shifts of ν_3, are listed in Table 2. For the cases where charge transfer occurred spontaneously, ν_3 is in the range of 2164−2182 cm^{-1} in HNCO complexes and 2189−2219 cm^{-1} in HOCN complexes. As the cluster size increases and coordination is completed in the CIP structures, the values of ν_3 for HNCO and HOCN exhibit a tendency to converge, until the difference is reduced to 21 cm^{-1} in the $12H_2O$ structures. However, the predictions for HNCO are always closer to the experimental value, differing at most by just 16 cm^{-1} for the $4H_2O$ through $12H_2O$ cases, while the differences for HOCN never fall below 37 cm^{-1}. While there appears to be a slight but real difference in the XCN frequency depending on whether NH_4^+ is coordinated to the O or N end of OCN^-, confirmation may require additional experimental studies. Further investigation of this issue will follow in the sections on $OCN^- - H_3O^+$ complexes

and isolated OCN^- cluster calculations; it will be analyzed in section 4.4.

The isotope shifts of ν_3 were compared against the experimental data reported by Bernstein et al.[46] In the experiment, isotopic substitution of C produced a large shift of 58 cm^{-1}, which is consistent with its role as the central atom of the asymmetric oscillation (and C being lighter than N and O). Our calculated results agree very well with the experimental value of the ^{13}C shift. The computed results for HNCO of 59−60 cm^{-1} for all of the clusters are in excellent agreement, while there is a slightly greater variation observed across the HOCN complexes, 54−60 cm^{-1}. All values of the ^{15}N shift for CIP cluster cases involving HNCO are smaller than the experimental value of 19 cm^{-1}, but they increase with cluster size. HOCN exhibits the opposite trend: all values overestimate the shift, but the error generally decreases with cluster size. For the ^{18}O isotope shifts, the behavior is reversed.

In contrast to the shifts for ^{13}C, ^{15}N, and ^{18}O, calculated deuterium shifts exhibited much larger fluctuations, including sign changes. While the experimental value of −8 cm^{-1} is a very small D shift, it is considered to be real.[46] For the HNCO complexes, the results are consistently in the correct direction for the most part, though the magnitude was as large as 44 cm^{-1}. For HOCN, half of the complexes showed positive deuterium shifts, and the deviations from the experimental value were also as large as 42 cm^{-1}. No consistent trends are discernible in the D shifts as a function of cluster size or other factors. The $12H_2O$ complexes produced the best agreement with the laboratory data, as reported in our preliminary paper.[40] In that study, we concluded on the basis of the absence of cluster-dependent trends and by performing partial substitutions in the largest clusters that the D shift is a delocalized effect. The large variations and the delocalization of the deuterium shift correspond well with the experimental study of Novozamsky et al.[50] who observed matrix-dependent D shifts.

Intensities for ν_3 are also shown in Table 2. Accurate intensities are critical for estimating the concentrations of molecular species in the ISM. The range of calculated intensities agrees to an order of magnitude with the value of the latest laboratory measurement by van Broekhuizen, Keane, and Schutte,[52] while agreement with values from previous experiments[30] is less satisfactory.

Finally, computed values for two additional weak bands of OCN^- are also given in Table 2: the symmetric stretching (ν_1) and bending (ν_2) modes. While they were corrected with a scaling factor specifically tuned for predicting ν_3, the agreement with the experimental data is generally satisfactory. The results for HNCO complexes are in better agreement with the experiment than those of HOCN complexes.

4.2. OCN^-−H_3O^+ CT Complexes: Can XCN Form without NH_3? It is well-known that strong acids are readily deprotonated in water. With pK_a values of about 3.5, HNCO and HOCN are both moderately strong organic acids. It is therefore of interest to investigate if OCN^-−H_3O^+ CT complexes can form as readily as OCN^-−NH_4^+. For this study, we built pure water complexes of both acids by replacing NH_3 with H_2O in the initial structures of the $12H_2O$ OCN^-−NH_4^+ complexes described previously. During optimization, proton transfer from both HNCO and HOCN to H_2O occurred spontaneously in these pure water complexes. A CIP structure formed at the beginning of the optimizations, but a second proton transfer occurred subsequently from H_3O^+ to a neighboring H_2O. The optimized complex arising from HOCN shown in Figure 4 is thus an SSP structure. Unlike the SSP structures for OCN^-−NH_4^+ CT complexes, where the entire NH_4^+ ion moves physically, here, a proton can readily hop from water to water. As in the NH_3 calculations described above, a similar structure was found for the HNCO case. However, the first proton transfer required significantly more optimization steps in the HNCO case (342 vs 4). Also, spontaneous transfer occurred in a HOCN−H_2O complex having only five additional H_2O molecules around them, while HNCO needs at least nine H_2O molecules for spontaneous deprotonation. As described in section 4.1, HOCN behaves as a stronger acid than HNCO. To date, no experimental ice studies have been performed with HOCN, but it appears that the XCN feature should develop at even colder temperatures in that case than it does for HNCO.

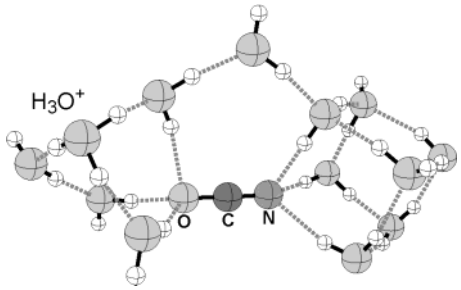

Figure 4. Optimized pure DFT structure for OCN^-−H_3O^+ from HOCN−H_2O solvated with 12 water molecules. A similar structure was obtained from HNCO−H_2O, with OCN^- reversed.

Frequency data for the $12H_2O$ OCN^-−H_3O^+ complexes are included in Table 2. The values of ν_1, ν_2, and ν_3 are similar to those of the $12H_2O$ CIP complexes with NH_4^+ present. The ν_3 values of 2187 and 2206 cm^{-1} for HNCO and HOCN, respectively, are only 5−6 cm^{-1} larger than the corresponding results for their NH_4^+ analogues, and again, they differ by about 20 cm^{-1}. The isotope shifts for C, N, and O exhibit almost the same values and trends as the $12H_2O$ complexes. The deuterium shifts, −10 and −9 cm^{-1} for HNCO and HOCN, respectively, are slightly different than the values for the $12H_2O$ OCN^-−NH_4^+ complexes, in keeping with the matrix dependence of D shifts described above and observed experimentally.[50] Further discussion of the similarities and differences in ν_3 and the isotope shifts and their dependence on the coordination and location of the cation can be found in section 4.4.

4.3. OCN^- with No Counterion. Previous sections examined the CIP and SSP structures of OCN^-−NH_4^+ and the SSP structures of OCN^-−H_3O^+. As a final case, we considered OCN^- in isolation, with no counterion present. An anion complex was built by replacing the NH_4^+ in the $12H_2O$ complex derived from HNCO with H_2O and then by adding two more water molecules to provide a roughly equivalent environment for both ends of the OCN^-. A second structure was also optimized in which the OCN^- was reversed. While very similar, the environments for the anion in the two forms are not quite the same. In particular, the orientation of the water molecule bridging the two cuboid units is reversed with respect to the OCN^-. A comparison of these two anion complexes allows us to observe the influence of subtly different electrostatic fields.

The optimized structure of the first anion complex described above is shown in Figure 5. Its detailed structure is very similar to the $12H_2O$ NH_4^+ and H_3O^+ complexes in bond lengths and charge separation. Also, the hydrogen bond lengths between OCN^- and the six coordinated waters fall in the range of 1.8−2.1 Å. The structure of the second, reversed case is nearly identical.

The frequencies and ν_3 isotope shifts for both of the $15H_2O$ OCN^- anion complexes are included in Table 2. The values of

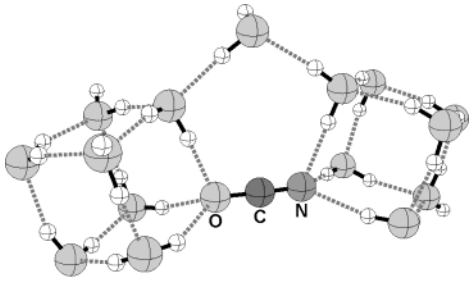

Figure 5. Optimized pure DFT structure for OCN^- with no counterion and solvated with 15 water molecules. A second structure was also optimized with OCN^- in the opposite orientation.

the asymmetric stretch are 2194 and 2184 cm^{-1}, which fall in the middle of those for the various HNCO and HOCN complexes. The difference of 10 cm^{-1} between the two values is evidently due to the orientation of the bridging water, with a small contribution from the caps.

The ^{13}C substitution effects are again consistent with other complexes. Isotope shifts for ^{18}O and ^{15}N follow the trends of HOCN and HNCO complexes, respectively, which were described in section 4.1. As in the large cluster calculations with a counterion present, one of the deuterium shifts (-6 cm^{-1}) for isolated OCN^- again agrees well with the measured value, while the other (-15 cm^{-1}) is off by a factor of about 2.

4.4. Modeling OCN^- Behavior in Ice: Cluster versus Counterion Effects. The previous three sections describe the structures and spectroscopic properties of various OCN^- complexes. By exploring a range of cluster sizes for the NH_4^+ case, we identified a configuration that provides full coordination around the ions. This was then employed to study the behavior of an alternate counterion (H_3O^+) as well as the case with no counterion. Together, there are six large cluster cases with a realistic coordination for a fully embedded OCN^- ion and differing counterion environments. In this section, we analyze commonalities and differences in these cases in order to evaluate how useful the cluster model is for evaluating subtle differences in behavior.

The agreement with experimental data for the vibrational properties of OCN^- in these large cluster cases is quite good. The value of the ν_3 band origin of 2181 cm^{-1} for the $12H_2O$ NH_4^+ complex derived from HNCO and NH_3 is the best of the six fully coordinated complexes. In addition, the computed ^{18}O, ^{15}N, ^{13}C, and D isotope shifts of ν_3 for this complex are mostly within $1-3$ cm^{-1} of their respective experimental values. As discussed in section 4.1, the D shift is very sensitive to the degree of coordination. While large fluctuations were shown in smaller complexes with less coordination, the variation in its value only ranges from -6 to -15 cm^{-1} in the six large cluster cases with full coordination, indicating that coordination is very important for this property.

The majority of the computed values for ν_3 are plotted together in Figure 6a as a function of the total number of moieties in each complex. Observing the general trend in ν_3, we find that the results clearly exhibit a dependence upon whether the parent molecule is HNCO or HOCN, as mentioned in section 4.1. Predictions for HOCN complexes are always higher than those for HNCO (by at least 21 cm^{-1}). This is true for both CIP and SSP structures, including the case where NH_4^+ is replaced with H_3O^+. Once proton transfer has occurred from HNCO or HOCN to form OCN^-, the only major distinction that remains is the location of the counterion. Although the maximum difference observed among the six large cluster values of ν_3 is just 25 cm^{-1}, counterion location evidently has an impact on the value of the OCN^- asymmetric stretching frequency.

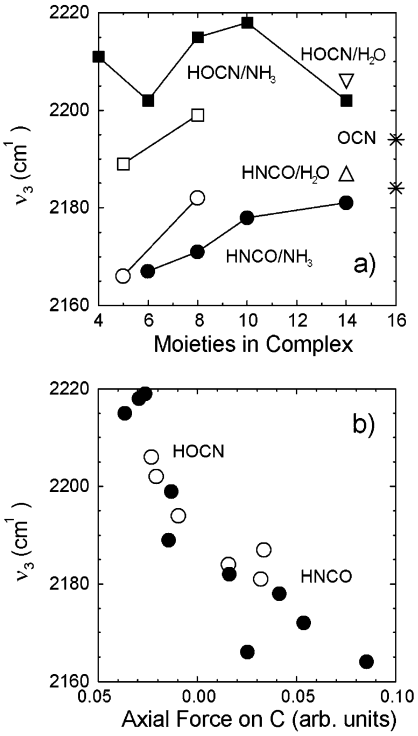

Figure 6. Behavior of the OCN^- asymmetric stretching frequency, ν_3. (a) Trends in ν_3 as a function of cluster size and the ion types. Solid symbols are contact ion pairs; open symbols are solvent-separated pairs. Cases: $OCN^-{-}NH_4^+$ from HNCO$-$$NH_3$ (○, ●) and from HOCN$-$$NH_3$ (□, ■); $OCN^-{-}H_3O^+$ from HNCO$-$$H_2O$ (△) and from HOCN/H_2O (▽); OCN^- with no counterion (*). (b) Force on the C atom in OCN^- parallel to the molecular axis due to the other moieties in the various complexes listed in Table 2, estimated by replacing atoms with computed mulliken charges. Open symbols correspond to the six fully coordinated structures described in the text.

TABLE 3: Estimated Axial Force Exerted on C in OCN^-

parents	structure type[a]	N[b]	F_{all}	F_{cation}
HNCO$-$$NH_3$	CIP	12	0.0321	0.0434
		8	0.0414	0.0404
		6	0.0537	0.0405
		4	0.0854	0.0401
	SSP	6	0.0162	0.0198
		3	0.0253	0.0131
HOCN$-$$NH_3$	CIP	12	−0.0207	−0.0371
		8	−0.0294	−0.0303
		6	−0.0366	−0.0271
		4	−0.0263	−0.0304
	SSP	6	−0.0131	−0.0145
		3	−0.0143	−0.0024
HNCO$-$$H_2O$	SSP	12	0.0335	0.0297
HOCN$-$$H_2O$	SSP	12	−0.0232	−0.0283
OCN^-	ION[c]	15	0.0157	
OCN^-	ION[c]	15	−0.0094	

[a] CIP: contact ion pair. SSP: solvent-separate pair. ION: isolated ion. [b] Number of waters added as solvent. [c] Two OCN^- anion complexes with nearly identical water structures were optimized.

However, the electrostatic field due to the water also makes a contribution, as indicated by the 10 cm^{-1} difference in ν_3 between the two anion structures, where no counterion was present. In general, while the counterion appears to decrease ν_3 slightly if it is closer to the N end of OCN^-, it appears to increase ν_3 by a small amount if it is closer to the O end.

Figure 6b adds weight to this argument. As an asymmetric oscillator, the ν_3 mode is dominated by the motion of the central C atom. The electrostatic force acting on C can be estimated

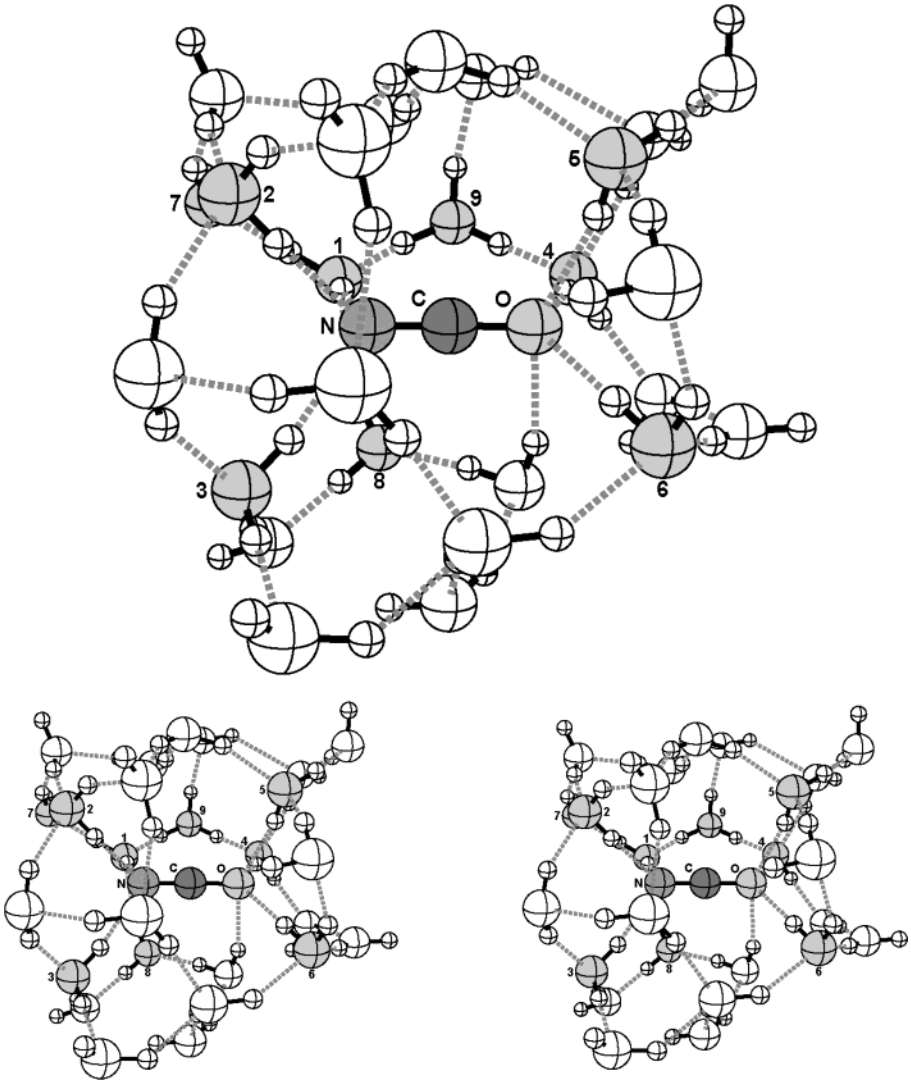

Figure 7. Optimized ONIOM structure and corresponding stereogram for deprotonation of HNCO. The model consisted of a high-level system composed of HNCO and nine waters treated with B3LYP/6-31+G** (numbered and shaded) coupled to a low-level system composed of HNCO and 27 waters treated with PM3.

by replacing the explicit atoms in each cluster with their respective computed Mulliken charges. The figure depicts the dependence of ν_3 on the component of the approximate net force acting parallel to the OCN^- axis (as listed in Table 3). The trend in Figure 6b is fairly well-defined: the shift in ν_3 is roughly proportional to the applied electrostatic force. The forces experienced by the O and N would be expected to exert an impact on ν_3, as well. Table 3 also shows the axial force contributions due to the cation alone. It is quite evident that the net force may also include a significant contribution from the water molecules (confirmed by the 10 cm^{-1} variation in the two anion cases described previously). All other things being equal, a nearby cation will likely influence the position of ν_3.

5. OCN^- Complex Formation Modeled with Explicit Water: ONIOM Treatment of HNCO Deprotonation in Pure Water

The prediction of spontaneous proton transfer from HNCO in pure water ice conflicts with the experimental observation[38,52] that no OCN^- peak appeared when HNCO was either co-deposited with H_2O at 10 K or deposited on a water ice surface, though the feature developed once the sample was warmed to 110 K in both cases.[38] While the discrepancy may be experimental in origin (arising from inhomogeneity during deposition, for example), there are theoretical issues to consider, as well. To investigate if our observation of spontaneous deprotonation is due to the limited cluster size and the somewhat strained hydrogen bonding interactions, we built a larger cluster model using ONIOM methodology. This extended model coupled a high-level model composed of HNCO and nine water molecules treated at the B3LYP/6-31+G** level with a low-level model consisting of HNCO and 27 water molecules treated with PM3. The high-level model system is an embedded subset of the low-level structure (see Figure 7). The ONIOM calculation behaved in the same manner as the pure DFT optimization described above: spontaneous deprotonation of HNCO was still observed, followed by a second proton transfer. The low-temperature threshold (110 K) for OCN^- formation observed by Raunier et al.[38] is indicative of a flat potential surface that possesses at most a very small reaction barrier. There may be sufficient methodological error present at the B3LYP/6-31+G** level to eliminate a barrier that might exist at a higher level of theory or with more complete basis sets. While the ONIOM calculation did not completely resolve the issue at hand, hybrid methodologies do provide a promising means of investigating extended

solvation systems; the ability to treat a sufficiently large portion of the model system via DFT is a critical component of this strategy.

6. Conclusion

Starting with simple IPCM and PCM models and advancing to extended DFT and ONIOM cluster calculations, we have investigated the behavior and properties of OCN^- charge-transfer complexes arising from HNCO or HOCN paired with NH_3 or H_2O in condensed-phase ice media. While the work confirms the experimental observation that HNCO and NH_3 can account for the XCN feature at 2165 cm^{-1}, it has demonstrated that a very similar spectroscopic feature can be produced with HOCN. Likewise, we have shown that either HNCO or HOCN should yield OCN^- without NH_3, with the HOCN case being more favorable. These predictions are amenable to experimental evaluation.

Despite yielding good values for the XCN feature, the PCM continuum solvent field method did not reproduce the full range of behavior exhibited by large cluster DFT calculations and did not accurately represent the D shift. PCM calculations can at least be used for initial explorations.

By including enough explicit water molecules to provide a coordination shell around the CT complex, cluster calculations were able to reproduce the characteristic vibrational frequencies of OCN^- and four isotope shifts in the dominant asymmetric stretching mode, ν_3. At the same time, the cluster approach appears to be sufficiently accurate to distinguish small shifts in ν_3 due to variations in the location of the counterion.

While it did not definitively resolve the conflict between theoretical prediction and the experimental observations for the deprotonation of HNCO in a pure water environment, the ONIOM model provides a means for building more realistic structures such as the hydrogen-bonded network in amorphous ice. The usefulness of hybrid models is only expected to improve as they become more sophisticated.

Our work and studies by other groups demonstrate that computational strategies and technology can address critical problems involving condensed-phase chemistry and spectroscopy, a capability with many important applications.

Acknowledgment. This study was supported by NASA Exobiology Grant NAG 5-13482. The authors thank Lou Allamandola, Scott Sandford, and Max Bernstein of NASA Ames Research Center for helpful conversations.

Supporting Information Available: Total energies (EB3LYP), zero-point energies (ZPE), and coordinates of all complexes using B3LYP/6-31+G** for seventeen complexes: eight complexes from HNCO, eight complexes from HOCN, and one OCN^- anion complex. This material is available free of charge via the Internet at http://pubs.acs.org.

References and Notes

(1) Cunningham, M. A.; Ho, L.; Nguyen, D. T.; Gillilan, R. E.; Bash, P. A. *Biochemistry* **1997**, *36*, 4800.
(2) Yokoyama, K.; Kawada, M.; Tamiya, E. *J. Electroanal. Chem.* **1997**, *434*, 217.
(3) Montoya, M.; Gouaux, E. *Biochim. Biophys. Acta* **2003**, *1609*, 19.
(4) Valdez, D.; Le Huerou, J. Y.; Gindre, M.; Urbach, W.; Waks, M. *Biophys. J.* **2001**, *80*, 2751.
(5) Livingstone, J. R.; Spolar, R. S.; Record, M. T. *Biochemistry* **1991**, *30*, 4237.
(6) Spolar, R. S.; Livingstone, J. R.; Record, M. T. *Biochemistry* **1992**, *31*, 3947.
(7) Gidalevitz, D.; Huang, Z. Q.; Rice, S. A. *Proc. Natl. Acad. Sci. U.S.A.* **1999**, *96*, 2608.
(8) Plumridge, T. H.; Waigh, R. D. *J. Pharm. Pharmacol.* **2002**, *54*, 1155.
(9) Poornima, C. S.; Dean, P. M. *J. Comput.-Aided Mol. Des.* **1995**, *9*, 513.
(10) Girardet, C.; Toubin, C. *Surf. Sci. Rep.* **2001**, *44*, 163.
(11) Goss, K. U.; Schwarzenbach, R. P. *Environ. Sci. Technol.* **1998**, *32*, 2025.
(12) Al-Abadleh, H. A.; Grassian, V. H. *Surf. Sci. Rep.* **2003**, *52*, 63.
(13) Deziel, E.; Comeau, Y.; Villemur, R. *Biodegradation* **1999**, *10*, 219.
(14) Rathbun, R. E. *Crit. Rev. Environ. Sci. Technol.* **2000**, *30*, 129.
(15) d'Hendecourt, L. B.; Allamandola, L. J.; Greenberg, J. M. *Astron. Astrophys.* **1985**, *152*, 130.
(16) Ball, P. *Nature* **2004**, *427*, 19.
(17) Lynden-Bell, R. M.; Rasaiah, J. C.; Noworyta, J. P. *Pure Appl. Chem.* **2001**, *73*, 1721.
(18) Woon, D. E. *Icarus* **1999**, *142*, 550.
(19) Woon, D. E. *Icarus* **2001**, *149*, 277.
(20) Woon, D. E. *J. Phys. Chem. A* **2001**, *105*, 9478.
(21) Woon, D. E. *Int. J. Quantum Chem.* **2002**, *88*, 226.
(22) Jenniskens, P.; Blake, D. F.; Wilson, M. A.; Pohorille, A. *Astrophys. J.* **1995**, *455*, 389.
(23) Smith, D. *Chem. Rev.* **1992**, *92*, 1473.
(24) Smith, D.; Spanel, P. *Mass Spectrom. Rev.* **1995**, *14*, 255.
(25) Herbst, E. *Annu. Rev. Phys. Chem.* **1995**, *46*, 27.
(26) Smith, D. *Int. J. Mass Spectrom. Ion Processes* **1993**, *129*, 1.
(27) Gudipati, M. S.; Allamandola, L. J. *Astrophys. J.* **2003**, *596*, L195.
(28) Woon, D. E. *Adv. Space Res.* **2004**, *33*, 44.
(29) Woon, D. E.; Park, J. Y. *Astrophys. J.* **2004**, *607*, 342.
(30) Demyk, K.; Dartois, E.; d'Hendecourt, L.; Jourdain de Muizon, M.; Heras, A. M.; Breitfellner, M. *Astron. Astrophys.* **1998**, *339*, 553.
(31) Grim, R. J. A.; Greenberg, J. M.; de Groot, M. S.; Baas, F.; Schutte, W. A.; Schimitt, B. *Astron. Astrophys., Suppl. Ser.* **1989**, *78*, 161.
(32) Soifer, B. T.; Puetter, R. C.; Russell, R. W.; Willner, S. P.; Harvey, P. M.; Gillett, F. C. *Astrophys. J.* **1979**, *232*, L53.
(33) Chiar, J. E.; Adamson, A. J.; Pendleton, Y. J.; Whittet, D. C. B.; Caldwell, D. A.; Gibb, E. L. *Astrophys. J.* **2002**, *570*, 198.
(34) Tegler, S. C.; Weintraub, D. A.; Allamandola, L. J.; Sandford, S. A.; Rettig, T. W.; Campins, H. *Astrophys. J.* **1993**, *411*, 260.
(35) Spoon, H. W. W.; Moorwood, A. F. M.; Pontoppidan, K. M.; Cami, J.; Kregel, M.; Lutz, D.; Tielens, A. G. G. M. *Astron. Astrophys.* **2003**, *402*, 499.
(36) Gibb, E. L.; Whittet, D. C. B.; Boogert, A. C. A.; Tielens, A. G. G. M. *Astrophys. J., Suppl. Ser.* **2004**, *151*, 35.
(37) Raunier, S.; Chiavassa, T.; Marinelli, F.; Allouche, A.; Aycard, J. P. *J. Phys. Chem. A* **2003**, *107*, 9335.
(38) Raunier, S.; Chiavassa, T.; Allouche, A.; Marinelli, F.; Aycard, J. P. *Chem. Phys.* **2003**, *288*, 197.
(39) Raunier, S.; Chiavassa, T.; Marinelli, F.; Allouche, A.; Aycard, J. P. *Chem. Phys. Lett.* **2003**, *368*, 594.
(40) Park, J. Y.; Woon, D. E. *Astrophys. J.* **2004**, *601*, L63.
(41) Grim, R. J. A.; Greenberg, J. M. *Astrophys. J.* **1987**, *321*, L91.
(42) Bernstein, M. P.; Sandford, S. A.; Allamandola, L. J. *Astrophys. J.* **1997**, *476*, 932.
(43) Lacy, J. H.; Baas, F.; Allamandola, L. J.; van de Bult, C. E. P. M.; Persson, S. E.; McGregor, P. J.; Lonsdale, C. J.; Geballe, T. R. *Astrophys. J.* **1984**, *276*, 533.
(44) Moore, M. H.; Donn, B.; Khanna, R.; A'Hearn, M. F. *Icarus* **1983**, *54*, 388.
(45) Palumbo, M. E.; Pendleton, Y. J.; Strazzulla, G. *Astrophys. J.* **2000**, *542*, 890.
(46) Bernstein, M. P.; Sandford, S. A.; Allamandola, L. J. *Astrophys. J.* **2000**, *542*, 894.
(47) Hudson, R. L.; Moore, M. H.; Gerakines, P. A. *Astrophys. J.* **2001**, *550*, 1140.
(48) Schutte, W. A.; Greenberg, J. M. *Astron. Astrophys.* **1997**, *317*, L43.
(49) Bernstein, M. P.; Sandford, S. A.; Allamandola, L. J.; Chang, S.; Scharberg, M. A. *Astrophys. J.* **1995**, *454*, 327.
(50) Novozamsky, J. H.; Schutte, W. A.; Keane, J. V. *Astron. Astrophys.* **2001**, *379*, 588.
(51) Palumbo, M. E.; Strazzulla, G.; Pendleton, Y. J.; Tielens, A. G. G. M. *Astrophys. J.* **2000**, *534*, 801.
(52) van Broekhuizen, F. A.; Keane, J. V.; Schutte, W. A. *Astron. Astrophys.* **2004**, *415*, 425.
(53) Nguyen-Q-Rieu; Henkel, C.; Jackson, J. M.; Mauersberger, R. *Astron. Astrophys.* **1991**, *241*, L33.
(54) Armstrong, J. T.; Barrett, A. H. *Astrophys. J., Suppl. Ser.* **1985**, *57*, 535.
(55) Snyder, L. E.; Buhl, D. *Astrophys. J.* **1972**, *177*, 619.
(56) Frisch, M. J.; Trucks, G. W.; Schlegel, H. B.; Scuseria, G. E.; Robb, M. A.; Cheeseman, J. R.; Zakrzewski, V. G.; Montgomery, J. A., Jr.; Stratmann, R. E.; Burant, J. C.; Dapprich, S.; Millam, J. M.; Daniels, A.

D.; Kudin, K. N.; Strain, M. C.; Farkas, O.; Tomasi, J.; Barone, V.; Cossi, M.; Cammi, R.; Mennucci, B.; Pomelli, C.; Adamo, C.; Clifford, S.; Ochterski, J.; Petersson, G. A.; Ayala, P. Y.; Cui, Q.; Morokuma, K.; Malick, D. K.; Rabuck, A. D.; Raghavachari, K.; Foresman, J. B.; Cioslowski, J.; Ortiz, J. V.; Baboul, A. G.; Stefanov, B. B.; Liu, G.; Liashenko, A.; Piskorz, P.; Komaromi, I.; Gomperts, R.; Martin, R. L.; Fox, D. J.; Keith, T.; Al-Laham, M. A.; Peng, C. Y.; Nanayakkara, A.; Gonzalez, C.; Challacombe, M.; Gill, P. M. W.; Johnson, B. G.; Chen, W.; Wong, M. W.; Andres, J. L.; Head-Gordon, M.; Replogle, E. S.; Pople, J. A. *Gaussian 98*, revision A.7; Gaussian, Inc.: Pittsburgh, PA, 1998.

(57) Sobolewski, A. L.; Domcke, W. *J. Phys. Chem. A* **2003**, *107*, 1557.

(58) Solcà, N.; Dopfer, O. *J. Am. Chem. Soc.* **2003**, *125*, 1421.

(59) Wysokiñski, R.; Michalska, D.; Bieñko, D. C. *J. Phys. Chem. A* **2003**, *107*, 8730.

(60) Clarke, T. M.; Gordon, K. C.; Officer, D. L.; Hall, S. B.; Collis, G. E.; Burrell, A. K. *J. Phys. Chem. A* **2003**, *107*, 11505.

(61) Choo, J.; Kim, S.; Drucker, S.; Laane, J. *J. Phys. Chem. A* **2003**, *107*, 10655.

(62) Ding, C. G.; Laasonen, K. *Chem. Phys. Lett.* **2004**, *390*, 307.

(63) Linstrom, P. J.; Mallard, W. G. NIST Chemistry WebBook. *NIST Standard Reference Database Number 69*. http://webbook.nist.gov. National Institute of Standards and Technology: Gaithersburg, MD (accessed March 2003).

(64) Miertus, S.; Scrocco, E.; Tomasi, J. *Chem. Phys.* **1981**, *55*, 117.

(65) Foresman, J. B.; Keith, T. A.; Wiberg, K. B.; Snoonian, J.; Frisch, M. J. *J. Phys. Chem.* **1996**, *100*, 16098.

(66) Becke, A. D. *J. Chem. Phys.* **1993**, *98*, 5648.

(67) Lee, C. T.; Yang, W. T.; Parr, R. G. *Phys. Rev. B: Condens. Matter* **1988**, *37*, 785.

(68) Hariharan, P. C.; Pople, J. A. *Theor. Chim. Acta* **1973**, *28*, 213.

(69) Clark, T.; Chandrasekhar, J.; Spitznagel, G. W.; Schleyer, P. V. *J. Comput. Chem.* **1983**, *4*, 294.

(70) Gibb, E. L.; Whittet, D. C. B.; Schutte, W. A.; Boogert, A. C. A.; Chiar, J. E.; Ehrenfreund, P.; Gerakines, P. A.; Keane, J. V.; Tielens, A. G. G. M.; van Dishoeck, E. F.; Kerkhof, O. *Astrophys. J.* **2000**, *536*, 347.

(71) The equilibrium barrier height is about 1.1 kcal/mol, with the CT complex 0.8 kcal/mol above the neutrals. However, when zero-point energy is included, the energy of the TS falls to 0.1 kcal/mol and the CT complex is at 2.3 kcal/mol, so the CT complex is not truly stable with just two waters.